Version of Record: https://www.sciencedirect.com/science/article/pii/S0264127518305148
Manuscript_948500260c1cbc39740f41dfb8abb48f

Effect of thermal annealing on stress relaxation and crystallization of ion beam sputtered amorphous $Si_{1-x}Ge_x$ thin films

F. Guo[1], M. Martyniuk[1], D. Silva[1], Y. Liu[2], K. Brookshire[1] and L. Faraone[1]

[1]Department of Electrical, Electronic and Computer Engineering, The University of Western Australia, Perth, WA 6009, Australia

[2]Department of Mechanical Engineering, The University of Western Australia, Perth, WA 6009, Australia

Abstract

$Si_{1-x}Ge_x$ ($0 \leq x \leq 1$) thin films were deposited by means of biased target ion beam sputtering at a low substrate temperature near 100 °C inside a vacuum chamber. The as-deposited films were all found to be amorphous and to be compressively stressed, and the magnitude of the compressive stress was found to decrease with increasing Ge content. Heat treatment for 30 minutes under vacuum conditions in the range from 100 °C to 800 °C was found to relax the compressive stress and to eventually cause crystallisation of the films at higher temperatures. The temperature required to achieve full stress relaxation was found to decrease with increasing Ge content, and to be well below that for film crystallisation. Annealing at temperatures above the crystallisation temperature caused physical damage to films containing more than 50 at %Ge. Films with < 50 at % Ge showed no damage after annealing up to 800 °C.

Keywords: SiGe, thin films, biased target sputtering, stress relaxation, annealing

1. Introduction

$Si_{1-x}Ge_x$ thin films have attractive optical and mechanical properties for application in optical microelectromechanical systems (MEMS) technologies. These include a high refractive index in the range of 3.6 to 4.2 [1], negligible absorption at infrared wavelengths [1], high mechanical strength, and suitable Young's modulus [2, 3] enabling $Si_{1-x}Ge_x$ to serve as an

optical and/or structural layer for free standing MEMS structures. Importantly, these materials are highly compatible with thin film and MEMS device fabrication technologies, such as chemical vapour deposition (CVD) or magnetron sputtering for thin film layer deposition, photo-lithography and etching for layer patterning, as well as integration with microelectronic circuits [4]. Owing to these characteristics, $Si_{1-x}Ge_x$ thin film materials have been widely incorporated in the fabrication of MEMS devices, such as the structural layers in pressure sensors [5, 6], functional films in thermoelectric gas sensors [7-9], base materials for heterojunction bipolar transistors [10, 11], thin film solar cells [12, 13], and electro-absorption modulators [14, 15].

Si and Ge have identical crystal structure and are fully miscible in the solid state to form alloys of any intermediate composition. $Si_{1-x}Ge_x$ thin films are commonly created by means of chemical vapour deposition from SiH_4 and GeH_4 precursors [16-20]. Advantages of the CVD method include low deposition temperatures (<490 °C) and high deposition rates [21], which produces Si-Ge thin films that are usually amorphous and hydrogenated, often denoted as a-SiGe:H [21-23]. Such films are amorphous, largely due to the low kinetic energy of the Si and Ge atoms at the low deposition temperature, and the hydrogen content in the films originates from the hydrogen-containing precursors, which can be as high as 6.8 at % [24]. Another common technique for fabricating $Si_{1-x}Ge_x$ thin films is physical sputtering, in which Si and Ge targets are bombarded by ionised atoms that are accelerated by either an electric or magnetic field, and eject the target material atoms towards a substrate surface for deposition as a thin film alloy. The source of ionised atoms is usually an inert gas, such as argon [25-27], and the Si-Ge thin films are usually amorphous and often contain ionised source atoms trapped within the films [28]. The films are amorphous because of the bombardment of the arriving atoms, whose high kinetic energy generally exceeds the threshold of atom displacement in the as-formed film, and causing random atom displacement and destruction of any atomic ordering. Both CVD and sputtered a-SiGe thin films can be crystallised by a post-deposition heat treatment at above 500 °C [21, 25, 27].

Many studies have been conducted to explore the properties of $Si_{1-x}Ge_x$ thin films. Gromova *et al.* studied the mechanical and electrical properties of hydrogenated microcrystalline silicon germanium (μc-$Si_{1-x}Ge_x$:H) thin films prepared by plasma enhanced CVD method, and found that the they contained low tensile stresses (25 MPa) and had relatively low electrical resistivities (7-9 mΩ•cm) compared to commercial bulk Si material [29]. Tajima *et al*. studied the thermoelectric properties of *radio frequency (RF)* sputtered $Si_{0.8}Ge_{0.2}$ thin

films for application in hydrogen gas sensors [7]. The amorphous $Si_{0.8}Ge_{0.2}$ layers were annealed at 850 °C in vacuum to achieve crystallisation, and exhibited a high carrier mobility of 10.54 cm^2/Vs and a high Seebeck coefficient of -198 μV/K (absolute value) [7]. The fabricated hydrogen sensor was able to detect hydrogen in air from 0.01% to 3% volume concentrations. Shahahmadi *et al*. studied Ge-rich SiGe thin films deposited by RF magnetron sputtering. The films were crystallised via annealing at 450 °C and were found to have a band gap of 1.2 – 1.26 eV, which is suitable for photovoltaic applications [30, 31]. In a separate work, the electrical resistance of ion beam sputtered $Si_{0.8}Ge_{0.2}$ thin films was measured to decrease by 80% as a result of electrical pulse annealing [32].

In addition to the above mentioned functional properties, the thin film mechanical properties and physical state are also important considerations for MEMS design [29, 33, 34]. One of the advantages of using SiGe in MEMS devices is the ability to control the Si/Ge ratio, which provides an additional avenue to control the properties of the resulting material. For example, the Young's modulus of a pure Si thin film is generally found to be ~180 GPa whereas that of pure Ge is ~ 140 GPa, which raises the possibility of fine tuning the Young's modulus of the alloy film between these two values by adjusting the alloy film composition [35, 36]. Schaffler has reported that the refractive index of $Si_{1-x}Ge_x$ thin films in the infrared region increases monotonically with Ge content, from 3.42 for x=0 to 4.00 for x=1 [36].

Some studies have investigated the internal stress and related crystallisation processes of $Si_{1-x}Ge_x$ ($0 \leq x \leq 0.6$) thin films [37-39]. Le Meur *et al.* found that ion beam sputtered $Si_{1-x}Ge_x$ thin films were highly compressively stressed in the as-deposited state (1~1.5 GPa) [37], which is commonly found in sputtered thin films. Therefore, when stress-free films are required, CVD techniques are often chosen in preference to sputtering. Sedyky *et al*. investigated CVD SiGe thin films prepared at elevated temperatures (>625 °C), under either atmospheric pressure or reduced pressure, and found that the films were polycrystalline and had residual stresses varying from -145 MPa (compressive) to +60 MPa (tensile) [38]. Control of residual stresses over such range is often desirable in MEMS fabrication. However, such high processing temperatures, and the even higher annealing temperatures often needed for film stress reduction, are not favorable for MEMS process integration [39, 40]. Also noteworthy, Tada *et al.* investigated crystallisation of CVD $Si_{1-x}Ge_x$ thin films prepared at temperatures below 400 °C and found that the required annealing crystallisation temperature decreased from 650 °C to 450 °C as the Ge content increased from 0% to 50% [41].

It is evident that both deposition conditions and post-deposition heat treatment can significantly alter the properties and the mechanical state of SiGe thin films. Whilst CVD SiGe thin films have been thoroughly investigated, much less is known of ion beam sputtered $Si_{1-x}Ge_x$ thin films. This study has investigated the effect of composition and the influence of post-deposition heat treatment on stress and crystallisation of $Si_{1-x}Ge_x$ thin films prepared by biased target ion beam deposition.

2. Experimental procedures

Si-Ge thin films of 500 nm nominal thickness were deposited onto (100) single crystal Si substrates by means of sputtering using a 4Wave Inc. biased target sputtering tool with an Kaufman type Ar ion beam source at a substrate temperature near 100 °C, as per the manufacturer's specification. The Si wafers were 90 μm thick and were cleaved into 20 mm×3 mm strips to use as substrates for deposition, with the [110] direction along the length of the samples. The film/substrate interface were prepared by standard solvent cleaning procedure. Si and Ge targets of 99.99% purity supplied by Super Conductor Materials, Inc. were used as elemental sources for deposition. Both targets are 4 inch diameter disks. The disk faces are arranged vertically to the ground, perpendicular to the ion source on top, and the two targets are 180 degree apart facing each other inside the chamber. The targets were sputtered simultaneously using deposition parameters listed in Table 1 under the same bias voltage of -800 V, but with different pulse times to allow control of film composition.

Table 1. Sample deposition parameters: target bias voltage = -800V, Ar flow rate = 53 sccm, target bias on/off time, film composition from EDS analysis, measured thin film thickness, Young's Modulus (E) and Hardness (H). Note that EDS analysis for film composition was normalised after excluding any Ar content.

Nominal film composition	Si target on/off time (μs)	Ge target on/off time (μs)	Thickness (nm)	EDS analysis	Ar (at.%)	Young's Modulus, E (GPa)	Hardness, H (GPa)
Si	12/2	OFF	528	Si	4.0	143	10.4
$Si_{0.7}Ge_{0.3}$	12/2	2/26	515	$Si_{0.73}Ge_{0.27}$	4.0	137	9.48
$Si_{0.5}Ge_{0.5}$	12/2	10/18	533	$Si_{0.49}Ge_{0.51}$	4.0	128	8.78
$Si_{0.3}Ge_{0.7}$	12/2	27/1	576	$Si_{0.28}Ge_{0.72}$	4.0	121	7.89

Ge	OFF	26/2	527	Ge	4.0	115	5.77

Thin film stress was determined by measuring the curvature of the film-substrate strip samples using a Zygo NewView 7300 optical surface profiometer, and calculated using the Stoney equation [42]. The curvature of each sample was measured both before and after deposition and the net change of the curvature was used for stress calculation.

All samples were annealed in vacuum (10^{-6} Torr) for 30 minutes to relax the internal stress of the films, using an ANNEALSYS AS-One rapid thermal annealing system with a new as-deposited sample used for each anneal. The heating rate was 20°C/s.

The thickness of the deposited films was measured using a Veeco Instruments Inc. Dektak 150 stylus profilometer. The morphology of the films was examined using a FEI Inc. Verios XHR scanning electron microscope (SEM), and the composition was analysed by means of X-ray energy-dispersive spectroscopy (EDS) within the SEM. All samples were coated with a 5 nm thick Pt layer to avoid charging effect under HRSEM. The crystallisation state of the films was determined by means of X-ray diffraction (XRD) using a PANalytical Inc. Empyrean diffractometer with Cu Kα radiation. A transmission electron microscope (FEI Titan G2 80-200 TEM/STEM) was used for examining the film structure and the Young's modulus and hardness of the films were measured using a Hysitron TI 950 TriboIndenter. The indentation was conducted under load control, and the load varied from 500 μN to 10000 μN.

3. Results and analysis

Figure 1 shows the as-deposited $Si_{0.5}Ge_{0.5}$ thin film sample, and the corresponding surface profilometry measurements of curvature. Figure 1(a) is an SEM image of the film, indicating no sign of defects, whereas the higher magnification in Figure 1(b) shows an "orange peel effect" surface texture due to the Pt coating used for SEM sample preparation and is not a feature of the underlying SiGe film [43]. The film surface is found to be perfectly flat and defect free, and Figure 1(c) shows Zygo profilometer images of the 20 × 3 mm strip sample. The left hand image is the surface of the bare Si wafer substrate before deposition, with the strip surface normal being along the [001] direction and the strip length along the [110] direction of the single crystal Si substrate. The central image shows the surface of the strip after deposition of the $Si_{0.5}Ge_{0.5}$ film (with the film side facing down). The right-hand colour

scale indicates the surface height and is common to both images. It is noted that the strip sample curves upwards, indicating a compressive stress in the film. Linear profiles of the sample were measured in both the longitudinal and lateral directions along the scan lines indicated in the profilometry image, as well as the radius of curvature calculated from these profiles.

Figure 1(d) shows the scan height profile of line A-A' (as indicated in Figure 1(c)) along the length of the strip sample and the local radii of curvature (determined within a ± 500 μm range on the profile at the point) along line A-A'. It is seen that the radii of curvature are largely the same at ~0.8 m along the full sample length. This implies that the sample profile is an arc of a circle, and that the stress is uniform along the length of the sample.

Figure 1(e) shows the height profiles and local radii of curvature along the lateral lines of BB', CC' and DD', as indicated in Figure 1(c). It is evident that the radii of curvature are also largely consistent for all the three scan lines, indicating the shape and stress uniformity. It is also notable that the radii of curvature along the width are marginally higher than along the length. Neglecting this small difference, the sample strip can be considered a biaxial system, thus the biaxial modulus is used in Stoney's equation to estimate film stress.

The above observations were found to be common for all samples, and independent of the Si-Ge composition. Using the radius of curvature data determined from bending profile measurements, film stresses were calculated using Stoney's equation for both the as-deposited films and after annealing at different temperatures. Figure 2 presents the determined stress of all films, plotted as a function of Ge content for different annealing temperatures in (a) and as functions of the annealing temperature for different film compositions in (b). It is evident that all $Si_{1-x}Ge_x$ thin films were compressively stressed in the as-deposited state, and that the magnitude of the compressive stress decreased with increasing Ge content from -650 MPa for x=0 to -300 MPa for x=1.

It was observed that annealing at elevated temperatures resulted in significant stress relaxation for all films, with most of the relaxation occurring at temperatures below 400 °C. The relative magnitude of the thin film compressive stress after annealing maintained the same trend with regard to Ge content as in the original as-deposited films (Figure 2(a)). Films annealed at higher temperatures eventually became near stress-free or slightly tensile (Figure 2(b)) and, in general, films with higher Ge content had higher internal tensile stress after annealing at high temperature.

The surface morphology of the films was examined using scanning electron microscopy. Figure 3 shows SEM micrographs of $Si_{0.7}Ge_{0.3}$ and $Si_{0.3}Ge_{0.7}$ after annealing. Figure 3(a) shows a $Si_{0.7}Ge_{0.3}$ film after anneal at 800 °C and (b) shows the same film at a higher magnification. The film is intact without any sign of damage in visible physical forms, which is practically the same for the Si film. Figures 3(c) and (d) show the $Si_{0.3}Ge_{0.7}$ film after annealing at 500 °C. This sample presented densely and uniformly distributed small damage holes. Similar surface damage was overserved on other high Ge content samples ($Si_{0.5}Ge_{0.5}$ and Ge) that are indicated by the arrows in the Figure 2(b).

The SEM images in Figure 4 show the progressive physical damage occurring in the $Si_{0.3}Ge_{0.7}$ sample after annealing at different temperatures, indicating that the physical damage commences at 500 °C, and the damage developed as small and uniformly distributed pin holes at lower temperatures into large semi-connected large voids at higher annealing temperatures.

It is also clear from the evidence presented above that there is a critical annealing temperature above which physical damage occurs in high Ge content films, as indicated by the arrows in Figure 2(b). It is observed that the critical annealing temperature decreases with increasing Ge content in the films and, no damage was observed for pure Si and $Si_{0.7}Ge_{0.3}$ films up to 800 °C, which was the maximum annealing temperature used.

The films were also analysed by means of grazing incident x-ray diffraction (GIXRD) with an incident angle of 0.8°. Figure 5 shows the GIXRD patterns of the five $Si_{1-x}Ge_x$ films before and after annealing at various temperatures. For each film composition, a new sample was used for each anneal. All films were amorphous in the as-deposited state. Annealing at elevated temperatures resulted in crystallization of the films, and additional samples were used for annealing at temperatures to narrow down the film crystallization temperature window to 10 °C. For clarity of presentation, films annealed at below the crystallization temperature window, which all remained amorphous, are not shown in the figure. It is seen that the critical temperature for crystallization decreases with increasing Ge content.

Figure 6 shows TEM analysis of the annealing-induced structural changes to the films. Figure 6(a) is a bright field TEM micrograph of a cross-section of the $Si_{0.3}Ge_{0.7}$ film annealed at 600 °C. The film structure is heterogeneous, with many isolated clusters in bright contrast to the surrounding continuous matrix. Figure 6(b) is a high resolution TEM image of a bright contrast region, labelled ‘A’ in Figure 6(a). The inset in (b) is the fast Fourier transform

pattern of the region, clearly indicating that these bright regions are amorphous $Si_{0.3}Ge_{0.7}$. Figure 6(c) shows a high resolution TEM image of the matrix of the film, as indicated by 'B' in Figure 6(a), and the inset in (c) shows the fast Fourier transform pattern of the region. It is evident the continuous region in the film was crystalline $Si_{0.3}Ge_{0.7}$. The compositions of the amorphous and crystalline regions were analyzed by means of EDS, and Figure 6(d) shows a high-angle annular dark-field (HAADF) image of the film cross section. In this image the isolated amorphous clusters appear in dark contrast. Figure 6(e) shows the element distribution along the line indicated in (d), as determined by EDS line scan with both Si and Ge registering very low x-ray counts within the amorphous regions. The significant signal drops are likely caused by void present in the amorphous regions, which could be a result of atoms interdiffusion or crystallisaiton upon annealing. Figure 6(f) plots the Si:Ge atomic ratio along the line which despite the strong signal difference between the amorphous and crystalline regions, remained essentially constant at 0.4 along the line, corresponding to the nominal Si:Ge = 3:7 molar composition of the film.

The mechanical properties of the SiGe films were determined by means of nanoindentation at the ambient temperature. The Young's modulus and hardness values obtained for each sample are the average values over 125 indents. Figure 7 shows the measured Young's modulus and hardness of the films, with (a) showing them as functions of the Ge content and (b) as a function of the annealing temperature for the $Si_{0.5}Ge_{0.5}$ film, which is representative of all samples. It is seen that both the Young's modulus and hardness decreased monotonically with increasing Ge content and that both parameters of each film show little variations after annealing at different temperatures.

4. Discussions

As presented in Figure 2(a), the as-deposited $Si_{1-x}Ge_x$ thin films all contained significant compressive stresses. This is consistent with previous observations of $Si_{1-x}Ge_x$ thin films prepared by ion beam sputtering [37], and the magnitude of the stress is generally higher than that found in $Si_{1-x}Ge_x$ thin films deposited by means of chemical vapour deposition [38, 44] or molecular beam epitaxy [45]. Compressive stress in these films is generally attributed to the effect of ion bombardment during sputtering [46], since particles arriving at the film surface, including both sputtered atoms and backscattered carrier ions, often have energy levels in the order of 10 eV to 100 eV [37]. These energy levels exceed the threshold energy needed for atomic displacement in $Si_{1-x}Ge_x$ films [47, 48], thus causing displacement of already deposited atoms within the film structure as well as forced entry of newly arriving

atoms. At the same time, the relatively low deposition temperature does not provide sufficient energy for dense atomic packing and relaxation of the structure via reshuffling of the atoms, leading to residual compressive stress [37, 46]. The magnitude of the stress is affected by several factors including ion energy, carrier ion flux, and properties of the target material [49, 50], as described the intrinsic stress scaling law [50]:

$$|\sigma| = 1.91 K j E_p^{0.5} Q / N_0 \quad (1)$$

where σ is the film stress, K is a scaling factor, j is the carrier ion flux, E_p is the carrier ion energy, N_0 is Avagadro's number, and Q is the elastic energy density of the film material, which is expressed as:

$$Q = \frac{YM}{(1-\nu)D} \quad (2)$$

where Y is the biaxial modulus, M is the atomic mass, ν is Poisson's ratio, and D is the density of the deposited film. In this work, all the parameters that determine stress in equation (1) are common for all film compositions, except Q. For the $Si_{1-x}Ge_x$ alloy, Q can be calculated as a function x, since as listed in Table 2 the Young's modulus, atomic mass, Poisson's ratio and density are all functions of x [3, 35, 36]. The calculated values of Q for $Si_{1-x}Ge_x$ are plotted as a function of Ge content in Figure 2(a), indicating that Q is negatively correlated with Ge content, and the relationship is consistent with the observed dependence of stress in as-deposited $Si_{1-x}Ge_x$ films.

Table 2. Young's modulus, atomic mass, Poisson's ratio, density and elastic energy of $Si_{1-x}Ge_x$ alloy as a function of x.

Properties	Equation	Source
Biaxial modulus, Y (GPa)	$Y = 180.45 - 39.96x$	[35], [36]
Atomic mass, M	$M = 28 \times (1 - x) + 32x$	Mass fraction
Poisson's ratios, ν	$\nu = 0.278 - 0.005x$	[3]
Density, D (g/cm^3)	$D = 2.329 + 3.493x - 0.499x^2$	[36]

Stress relaxation upon annealing has been observed previously in amorphous $Si_{1-x}Ge_x$ thin films [37, 51, 52]. Le Meur *et al.* reported that ion beam sputtered $Si_{0.97}Ge_{0.03}$ thin films

deposited at 550 °C had a compressive stress of 1 GPa, which can be reduced to 0.5 GPa by annealing at 750 °C for 15 minutes in flowing N_2 [37]. Kannan *et al.* investigated PECVD $Si_{1-x}Ge_x$ thin films and found that the stress of a $Si_{0.8}Ge_{0.2}$ film changed from compressive to tensile after annealing at 520 °C in N_2[52]. This stress relaxation has been attributed to reshuffling of atoms in the films at elevated temperature [52-55]. During annealing, "over packed" compressively stressed amorphous films may undergo structural relaxation involving short range movement and ordering of atoms, and annihilation of point defects inside the film structure [56, 57]. These atomic movements are generally described by material viscous flow, as suggested by Loopstra *et al.* and Witvrouw *et al.* [55, 58]:

$$\frac{\dot{\sigma}}{Y_f} = -\frac{\sigma}{6\eta} \tag{3}$$

where Y_f is the biaxial modulus of the film, η is the instantaneous shear viscosity, σ is the film stress and $\dot{\sigma}$ is the stress relaxation rate. The film viscosity can be calculated as [54, 58]:

$$\eta = \frac{\sigma}{6\varepsilon_p} \tag{4}$$

where ε_p is the biaxial plastic strain of the film. Since the film is constrained by the substrate in all lateral directions, then:

$$\varepsilon_p + \varepsilon_e = constant \tag{5}$$

$$\dot{\varepsilon_p} + \dot{\varepsilon_e} = 0 \tag{6}$$

where ε_e is the biaxial elastic strain of the film. Also, it is well-known that:

$$\dot{\varepsilon_e} = \frac{\dot{\sigma}}{Y_f} \tag{7}$$

By combining equations (4)-(7), equation (3) can be obtained. It has also been shown that viscosity is inversely proportional to defect density in amorphous Si and Ge films [53], thus η is expected to increase with time during the process of annealing as defects get progressively annihilated. In addition, relaxation reduces the value of σ. Therefore, according to equation (3), $\dot{\sigma}$ is expected to decrease continuously with time during annealing, which is consistent with the experimental observations shown in Figure 2.

Based on above argument, the limit to stress relaxation is expected to result in zero stress in the film, although experiments indicate that some films have become clearly tensile after annealing. This cannot be explained by structural relaxation via viscous atomic flow in the films, and may be attributed to the difference in coefficient of thermal expansion (CTE)

between the film and the silicon substrate, such that films with high Ge content will have higher CTE values than the silicon substrate [59]. The film stress is expected to fully relax to nil via atomic movement at the higher annealing temperatures, but during the period of post-annealing cooling to ambient, films with higher CTE values will contract more than the substrate does, resulting in tensile stresses in these films.

Closer examination of the XRD patterns shown in Figure 5 reveals that the positions of the three major peaks shift towards lower 2θ values for films with higher Ge contents as a result of annealing. Considering that all the films were near stress free after annealing, this diffraction peak shift implies a lattice constant increase with increasing Ge content, which is consistent with our expectation given that Ge is a larger atom than Si. Figure 8 plots the lattice constant determined using the 111 peak as a function of Ge content for the films annealed at 700 °C (400 °C for the pure Ge film). The lattice constant was also calculated using the 220 and 311 diffraction peaks, and the results are consistent with that from the 111 peak. It is evident that the lattice constant increased approximately linearly with increasing Ge content, as expected for the larger atomic size of Ge. Also plotted in the figure is the full width at half maximum (FWHM) of the 111 peak, as an indication of the crystallite size, which is found to decrease with increasing Ge content. This observation suggests that samples with higher Ge contents tend to have larger average crystal size for the same annealing temperature.

It is clear from the evidence presented above that the films exhibit different critical temperatures for various events upon annealing. Figure 9 plots these critical temperatures as a function of Ge content, including the lower and upper bound temperatures for crystallization, the temperature for full stress relaxation and the temperature for onset of physical damage. It is seen that all three characteristic temperatures decrease with increasing Ge content, and that the events follow the temperature sequence of stress relaxation-crystallization-physical damage upon annealing.

The deposited films are not suitable for MEMS applications due to the high compressive stress. However, the $Si_{0.3}Ge_{0.7}$ film can reach near stress free state after annealing at around 300 °C. This characteristic makes the film a suitable structure material in the MEMS devices applications. The low process temperature allows the integration of MEMS devices on prefabricated complementary metal-oxide-semiconductors (CMOS) as well as polymer substrates, such as benzocyclobutene, polyimide and polyethylene terephthalate [4].

5. Conclusions

(1) $Si_{1-x}Ge_x$ ($0 \leq x \leq 1$) thin films were deposited onto (100) single crystal silicon wafer substrates by biased target ion beam sputtering. Both Young's modulus and hardness of the films were found to monotonically decrease with increasing Ge content. High compressive stress was observed for all as-deposited $Si_{1-x}Ge_x$ films, and the magnitude of the stress was found to decrease with increasing Ge content.

(2) Annealing in vacuum was found to cause changes to the films, including stress relaxation, crystallization and, in some cases, physical damage. The low Ge-content films became stress free after annealing, whereas in high Ge-content films the stress became slightly tensile after annealing at high temperature.

(3) High Ge-content films were also found to be more susceptible to physical damage upon high temperature annealing. The damage occurs in the form of small and randomly distributed holes and voids in the films.

(4) The critical temperatures required for stress relaxation, crystallization, and the onset of physical damage were all found to decrease with increasing Ge content. The lattice constant of the crystallized films was also found to increase linearly with Ge content. The occurrence of the three events appear to follow a consistent order of stress relaxation - crystallisation – physical damage upon annealing in vacuum.

Acknowledgement

We acknowledge financial support from the Australian Research Council in grants DP140101766 and LE150100006, and the technical and in-kind support of the Office of Science of the WA State Government, Western Australian Node of the Australian National Fabrication Facility and Australian Microscopy & Microanalysis Research Facility at the Centre for Microscopy, Characterisation & Analysis of The University of Western Australia, facilities funded by the University, State and Commonwealth Governments.

References

[1] M.K. Bhan, L.K. Malhotra and S.C. Kashyap, “Electrical and optical properties of hydrogenated amorphous silicon-germanium (a-$Si_{1-x}Ge_x$) film prepared by reactive ion beam sputtering”, *J. Appl. Phys*., 66, 2528, 1989.

[2] S. Sedky, P. Fiorini, M. Caymax, S. Loreti, K. Baert, L. Hermans and R. Mertens, “Structural and mechanical properties of polycrystalline silicon germanium for micromachining applications”, *Journal of Microelectromechanical Systems*, 7, 365-372, 1998.

[3] J.J. Wortman and R.A. Evans, “Young’s Modulus, Shear Modulus, and Poisson’s Ratio in Silicon and Germanium”, *J. Appl. Phys.*, 36, 153, 1965.

[4] J. El-Rifai, S. Sedky, R.V. Hoof, S. Severi, D. Lin, S. Sangameswaran, R. Puers, C.V. Hoof and A. Witvrouw, “SiGe MEMS at processing temperature below 250°C”, *Sens. Actuators*, 188, 230-239, 2012.

[5] A. D. Sundararajan and S. M. R. Hasan, "Elliptic Diaphragm Capacitive Pressure Sensor and Signal Conditioning Circuit Fabricated in SiGe CMOS Integrated MEMS," *IEEE Sensors Journal*, 15, 1825-1837, 2015.

[6] Y. G. S. S. Sai Charan and A. D. Sundararajan, “Integrated MEMS Capacitive Pressure Sensor with On-Chip CDC for a Wide Operating Temperature Range”, *Nanoelectronic Materials and Devices*, 466, 61-79, 2018.

[7] K. Tajima, F. Qiu, W. Shin, N. Sawaguchi, N. Izu, I. Matsubara and N. Murayama, “Thermoelectric properties of RF-Sputtered SiGe Thin Film for Hydrogen Gas Sensor”, *Japanese Journal of Applied Physics*, 43, 5978-5983, 2004.

[8] T. Goto, T. Itoh, T. Akamatsu, Y. Sasaki, K. Sato and W. Shin, “Heat transfer control of micro-thermoelectric gas sensor for breath gas monitoring”, *Sens. Actuators B: Chemical*, 249, 571-580, 2017.

[9] N. Rothbart, K. Schmalz, J. Borngräber, S. Berk Yilmaz, D. Kissinger and H. W. Hübers, “Towards breath gas detection with a 245 GHz gas sensor based on SiGe BiCMOS technology”, *2017 IEEE SENSORS*, Glasgow, 2017, pp. 1-3.

[10] G.G. Fischer and G. Sasso, “Ageing and thermal recovery of advanced SiGe heterojunction bipolar transistors under long-term mixed-mode and reverse stress conditions”, *Microelectronics Reliability*, 55, 498-507, 2015.

[11] V. Huard *et al*., "Key parameters driving transistor degradation in advanced strained SiGe channels," *2018 IEEE International Reliability Physics Symposium (IRPS)*, Burlingame, CA, 2018, pp. P-TX.4-1-P-TX.4-6.

[12] X. Zhao, D. Li, B. Conrad, L. Wang, A.H. Soeriyadi, M. Diaz, A. Lochtefeld, A. Gerger, I. Perez-Wurfl and A. Barnett, "Material and device analysis of SiGe solar cell in a GaAsP-SiGe dual junction solar cell on Si substrate", *Solar Energy Materials and Solar cells,* 134, 114-121, 2015.

[13] S. Hussain, H. Mehmood, M. Khizar and R. Turan, "Design and analysis of an ultra-thin crystalline silicon heterostructure solar cell featuring SiGe absorber layer", *IET Circuits, Device & Systems,* 2018.

[14] J. Gao, J. Sun, J. Jiang, H. Zhou and Y. Zhou, "Design and analysis of electro-absorption modulators with uniaxially stressed Ge/SiGe multiple quantum wells", *Optics Express,* 25, 10874-10884, 2017.

[15] L. Mastronardi, M. Banakar, A.Z. Khokhar, N. Hattasan, T. Rutirawut, T. Domínguez Bucio, K. M. Grabska, C. Littlejohns, A. Bazin, G. Mashanovich, and F.Y. Gardes, "High-speed Si/GeSi hetero-structure Electro Absorption Modulator," *Opt. Express*, 26, 6663-6673, 2018

[16] A.A. Shklyaev, V.I. Vdovin, V.A. Volodin, D.V. Gulyaev, A.S. Kozhukhov, M. Sakuraba and J. Murota, "Structure and optical properties of Si and SiGe layers grown on SiO_2 by chemical vapor depositon", *Thin Solid Films,* 579, 131-135, 2015.

[17] Y. Yamaoto, P. Zaumseil, G. Capellini, M.A. Schubert, A. Hesse, M. Albani, R. Bergamaschini, F. Montalenti, T. Schroeder and B. Tillack, "A self-ordered, body-centered tetragonal superlattice of SiGe nanodot growth by reduced pressure CVD", *Nanotechnology,* 28, 485303, 2017.

[18] Y. Kim, S. Yoon, D. Ko and H. Sohn, "Influence of Si precursor type on the surface roughening of SiGe epitaxial layers deposited by ultrahigh vacuum chemical vapor deposition method", *Journal of Vacuum Science & Technology A: Vacuum, Surfaces, and Film,* 35, 041403, 2017.

[19] J.E. Halpin, S.D. Rhead. A.M. Sanchez, M. Myronov and D.R. Leadley, "Growth of complex SiGe/Ge superlattices by reduced pressure chemical vapour deposition at low temperature", *Semiconductor Science and Technology,* 30, 114009, 2015

[20] D. Qi, H. Liu, D. Huang, L. Wang, S. Chen and C. P. Grigoropoulos, "High-quality strain-relaxed $Si_{0.72}Ge_{0.28}$ layers grown by MBE-UHV/CVD combined deposition chamber", *Journal of Alloys and Compounds*, 735, 588-593, 2018.

[21] S. Joseph, N. Saraf, A. Umamaheswara, V. Madakasira and N. Bhat, "Role of thermal annealing on SiGe thin films fabricated by PECVD", *Materials Science in Semiconductor Processing*, 40, 655-663, 2015.

[22] D. P. Pham, S. Kim, A. H. T. Le, J. Park and J. Yi, "Diminished band discontinuity at the p/i interface of narrow-gap a-SiGe:H solar cell by hydrogenated amorphous silicon oxide buffer layer", *Journal of Alloys and Compounds*, 762, 616-620, 2018.

[23] L.W. Veldhuizen, C.H.M. van der Werf, Y. Kuang, N.J. Bakker, S.J. Yun and R.E.I. Schropp, "Optimization of hydrogenated amorphous silicon germanium thin films and solar cells deposited by hot wire chemical vapour deposition", *Thin Solid Films*, 595, 226-230, 2015.

[24] P. Sladek, V. Bursikova and P. Stahel, "Structural and defect changes of hydrogenated SiGe films due to annealing up to 600°C", *Phys. Status Solidi*, 7, 820-823, 2010.

[25] W.K. Choi, L.K. The, L.K. Bera and W.K. Chim, "Microstructural characterization of rf sputtered polycrystalline silicon germanium films", *J. Appl. Phys.*, 91, 444, 2002.

[26] S. Ke, S. Ye, J. Yang, Z. Wang, C. Wang and Y. Yang, "Morphological evolution of self-assembled SiGe islands based on a mixed-phase pre-SiGe island layer grown by ion beam sputtering depostion", *Applied Surface Science*, 328, 387-394, 2015.

[27] E.V. Jelenkovic, K.Y. Tong and Z. Sun, "Properties of crystalized $Si_{1-x}Ge_x$ thin films deposited by sputtering", *J. Vacuum Science & Technology*, 15, 2836, 1997.

[28] M. Serenyi, J. Betko, A. Nemcsics, N.Q. Khanh and M. Morvic, "Fabrication of a-SiGe structure by rf sputtering for solar cell puerposes", *phys. stat. sol.*, 3, 857-861, 2003.

[29] M. Gromova, K. Baert, C. Van Hoof, A. Mehta and A. Witvrouw, "The novel use of low temperature hydrogenated microcrystalline silicon germanium (μcSiGe:H) for MEMS applications", *Microelectronic Engineering*, 76, 266-271, 2004.

[30] S.A. Shahahmadi, A.A. Zulkefle, A.K.M. Hasan, S.M. Rana, B. Bais, M. Akhtaruzzaman, A.R.M. Alamoud and N. Amin, "Ge-rich SiGe thin film deposition by co-sputtering in in-situ and ex-situ phase crystallization for photovoltaic applications", *Materials Science in Semiconductor Processing*, 56, 160-165, 2016.

[31] S.A. Shahahmadi, B. Yehaneh, N. Huda, N. Asim, M. Hafidz, M.M. Alam, Z.A. Alothman, K. Sopian and N. Amin, "Properties of a-SiGe Thin Films on Glass by Co-sputtering for Photovoltaic Absorber Application", *J. Nanosci. Nanotechnol*., 15, 9275-9280, 2015.

[32] P. Pichanusakorn, N.B. Elsner and P.R. Bandaru, "Increasing electrical conductivity in sputter-deposited Si/SiGe multilayers through electrical pulse based annealing", *Electronics Letters*, 44, 1274-1275, 2008.

[33] M. Martyniuk, J. Antoszewski, C. A. Musca, J. M. Dell and L. Faraone, "Stress in low-temperature plasma enhanced chemical vapour deposited silicon nitride thin films", *Smart Mater. Struct.*, 15, 29-38, 2006.

[34] S. Mertin, B. Heinz, O. Rattunde, G. Christmann, M. Dubois, S. Nicolay and P. Muralt, "Piezoelectric and structural properties of c-axis textured aluminium scandium nitride thin films up to high scandium content", *Surface and Coatings Technology*, 343, 2-6, 2018

[35] M. Hopcroft, "What is Young's Modulus of Silicon?" *Journal of Microelectromechanical Systems*, 19, 229-238, 2010.

[36] F. Schaffler, *Properties of Advanced SemiconductorMaterials GaN, AlN, InN, BN, SiC, SiGe.* Eds. Levinshtein M.E., Rumyantsev S.L., Shur M.S., John Wiley & Sons, Inc., New York, 2001, 149-188.

[37]Y. Le Meur, F. Meyer, C. Pellet, C. Schwebel, P. Moller, A. Buxbaum, A. Raizman and M. Eizenberg. "Stress in $Si_{1-x}Ge_x$ films prepared by ion sputtering: origin and relaxation", *Thin Solid Films*, 222, 180-183, 1992.

[38] S. Sedky, P. Fiorini, M. Caymax, S. Loreti, K. Baert, L. Hermans and R. Mertens, "Structureal and Mechanical Properties of Polycrystalline Silicon Germanium for Micromachining Applications", *Journal of Microelectromechanical Systems*, 7, 365-372, 1998.

[39] S. Chang and S. Sivoththaman, "Development of a low temperature MEMS process with a PECVD amorphous silicon structural layer", *J. Micromech. Microeng*, 16, 1307-1313, 2006.

[40] A.E. Franke, J.M. Heck, T. King and R.T. Howe, "Polycrystalline Silicon-Germanium Films for Integrated Microsystems", *Journal of Microelectromechanical Systems*, 12, 160-171, 2003.

[41] M. Tada, J. Park, J.R. Jain and K.C. Saraswat, “Low-Temperature, Low-Pressure Chenical Vapor Deposition and Solid Phase Crystallization of Silicon-Germanium Films”, *Journal of Electrochemical Society*, 156, D23-D27, 2009.

[42] G.G. Stoney, “The tensions of metallic films deposited by electrolysis”, *Proc. R. Soc. Land*., 82, 172-175, 1909.

[43] Y. Liu, N. Jehanathan, H. Yang, J. Laeng, “SEM observation of the “orange peel effect” of materials”, *Materials Letters*, 61, 1433-1435, 2007.

[44] D. Depla and B.R. Braeckman, “Quantitative correlation between intrinsic stress and microstructure of thin films”, *Thin Solid Films*, 90-93, 2016.

[45] J.C. Bean, L.C. Feldman, A.T. Fiory, S. Nakahara and I.K. Robinson, “Ge_xSi_{1-x}/Si strained-layer superlattice grown by molecular beam epitaxy”, *J. Vac. Sci. Technol. A*, 2, 322, 1984.

[46] F. M. D’Heurle, “Aluminum films deposited by rf sputtering”, *Metallurgical and Mterisals Transactions B*, 1, 725-732, 1970.

[47] J. Lefevre, J.M. Costantini, S. Esnouf and G. Petite, “Silicon threshold displacement energy determined by photoluminescence in electron-irradiated cubic silicon carbide”, *J. Appl. Phys.*, 105, 2009.

[48] E. Holmstrom, K. Nordlund and A. Kuronen, “Threshold defect production in germanium determined by density functional theory molecular dynamics simulations”, *Physica Scripta*, 81, 2010.

[49] B.R. Braeckman and D. Depla, “On the amorphous nature of sputtered thin film alloys”, *Acta Materialia*, 323-329, 2016.

[50] H. Windischmann, “An intrinsic stress scaling law for polycrystalline thin films prepared by ion beam sputtering”, *J. Appl. Phys.* 62, 1800-1807, 1987.

[51] J. A. Floro, P.G. Kotula, S.C. Seel and D.J. Srolovitz. “Origins of Growth Stresses in Amorphous Semiconductor Thin Films”, *Physical Review Letters*, 91, 9, 2003.

[52] S. Kannan, C. Taylor and D. Allred, “PECVD growth of Si_x:Ge_{1-x} films for high speed devices and MEMS”, *Journal of Non-Crystalline Solids*, 352, 1272-1274, 2006.

[53] A. Witvrouw and F. Spaepen, “Viscosity and elastic constants of amorphous Si and Ge”, *J. Appl. Phys.*, 74, 7154-7161, 1993.

[54] F.A. McClintock and A.S. Argon, *Mechanical Behavior of Material,* MA: Addison-Wesley, Chap. 7. 1966.

[55] O.B. Loopstra, E.R. van Snek, Th. H. de Keijser and E.J. Mittemeijer, "Model for stress and volume changes of a thin film on a substrate upon annealing: Application to amorphous Mo/Si multilayers", *Phys. Rev. B.,* 44, 13519-13533, 1991.

[56] F. Spaepen, R. Balian, M. Kleman and J. P. Poirier, *Physics of Defects, Les Houches session XXXV,* North Holland, Amsterdam, p. 737, 1984

[57] S. Roorda, W.C. Sinke, J.M. Poate, D.C. Jacobson, S. Dierker, B.S. Dennis, D.J. Eaglesham, F. Spaepen and P. Fuoss"Structural relaxation and defect annihilation in pure amorphous silicon", *Phys. Rev. B.* 44, 13519-13530, 1991.

[58] A. Witvrouw and F. Spaepen, "the viscosity of amorphous Pd-Si and Pd-Si/Pd-Si-Fe multilayers determined from stress relaxation in thin films on a substrate", *J. Appl. Phys.,* 75, 1456-1462, 1994.

[59] *V. V. Zhdanova*, M.G. *Kakna,* T.Z. *Samadashvili*, *A.* Izv, *Nauk. Neorg. Mater. 3,* 1263, *1967.*

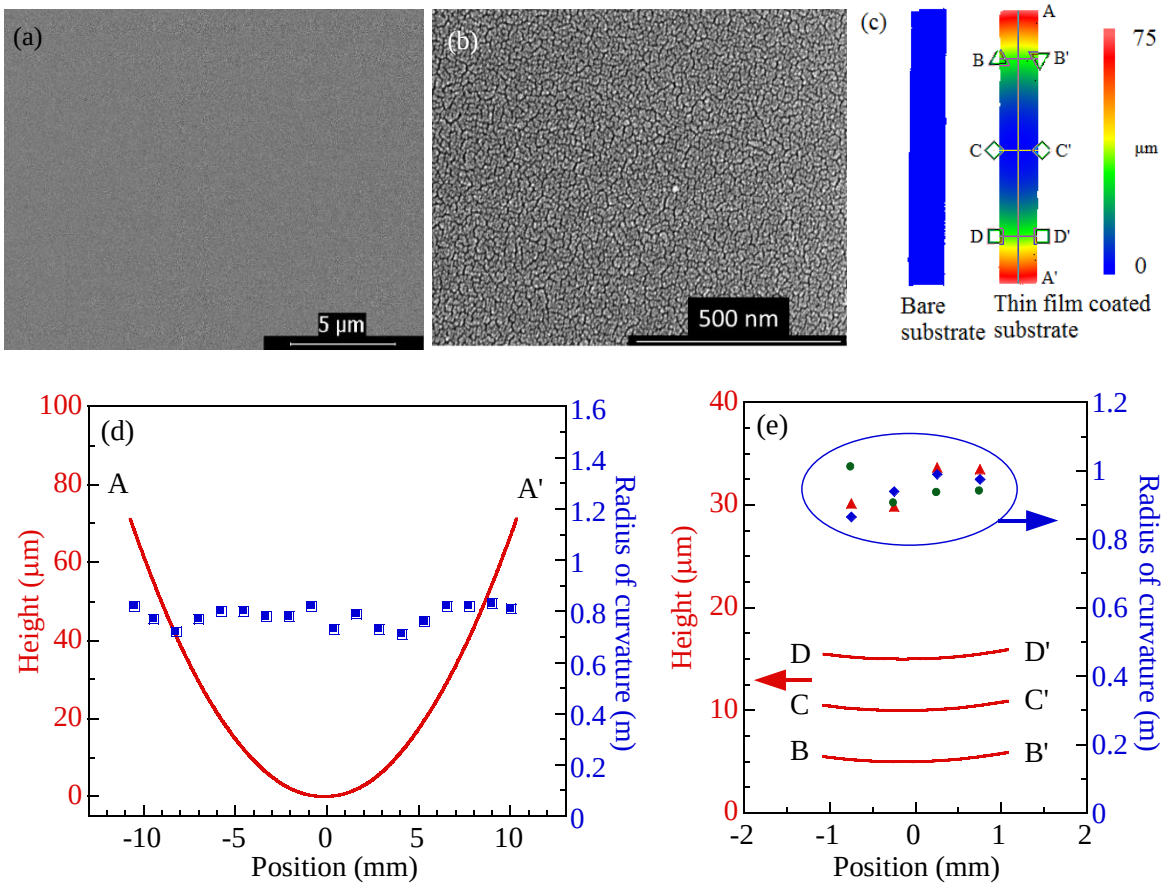

Figure 1. A $Si_{0.5}Ge_{0.5}$ film and film stress measurement. (a) and (b): SEM images of the film in as-deposited condition. (c): Zygo images of the surface profile measurement of the 20 mm × 3 mm strip sample before and after film deposition. (d): Height profile (curve, left axis) and radius of curvature (data points, right axis) along the length of the strip sample. (e): Height profile (curve, left axis) and radius of curvature (data points, right axis) along the width at three different locations of the strip sample. The positions of the surface profiles across the width of the sample have been offset vertically for clarity of presentation.

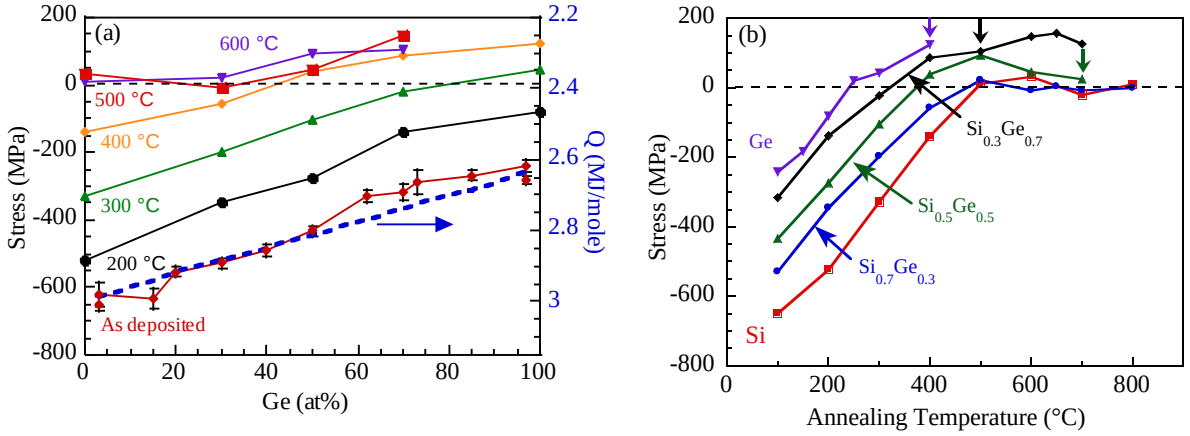

Figure 2. Effects of Ge content and annealing temperature on film stress. For the as-deposited films in (a), each data point represents one deposition event consisting of 3-4 samples, and the dashed line presents the calculated elastic energy density (Q) of $Si_{1-x}Ge_x$ thin films plotted as a function of Ge content on the right-hand Y axis (note the reverse order on the second Y axis). The arrows in (b) indicate the critical temperatures at which film surface damage was observed in samples with higher Ge content.

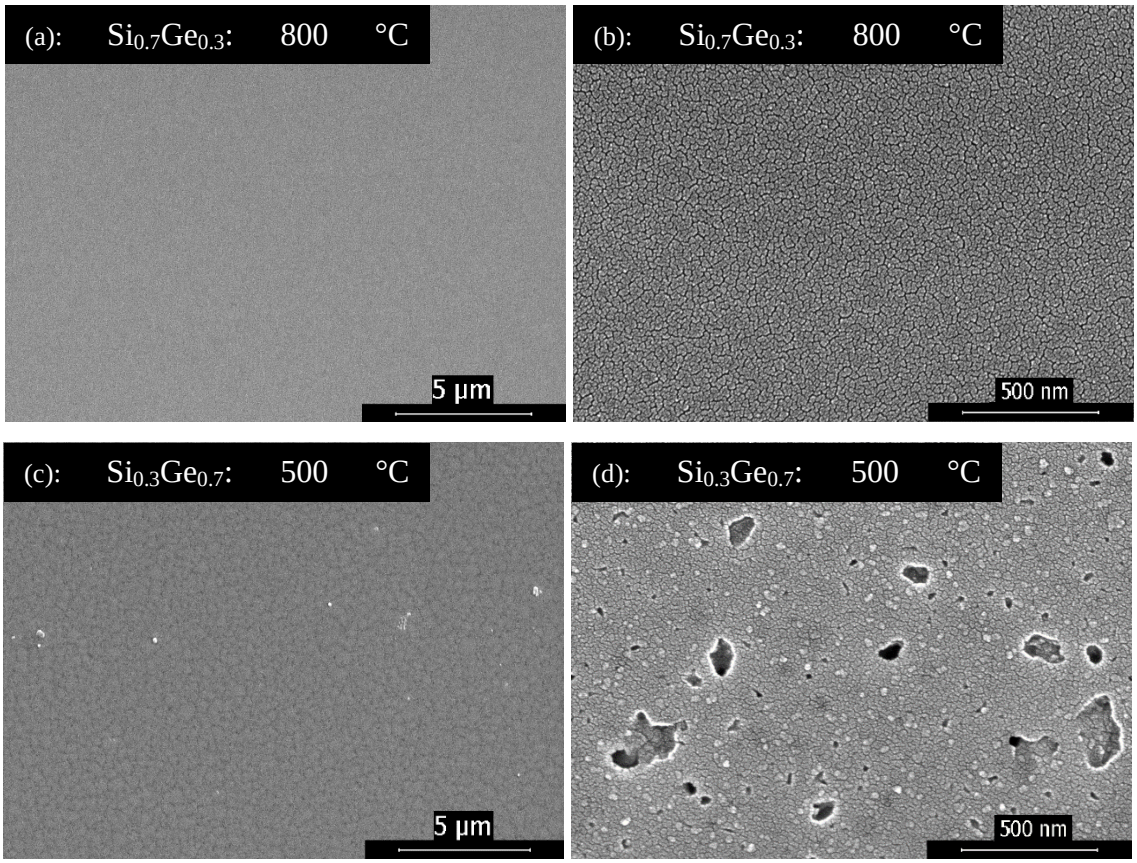

Figure 3. Effect of vacuum annealing on $Si_{1-x}Ge_x$ thin film morphology. (a) and (b): A $Si_{0.7}Ge_{0.3}$ film annealed at 800 °C. (c) and (d): A $Si_{0.3}Ge_{0.7}$ film annealed at 500 °C. Note the different magnification scales between images.

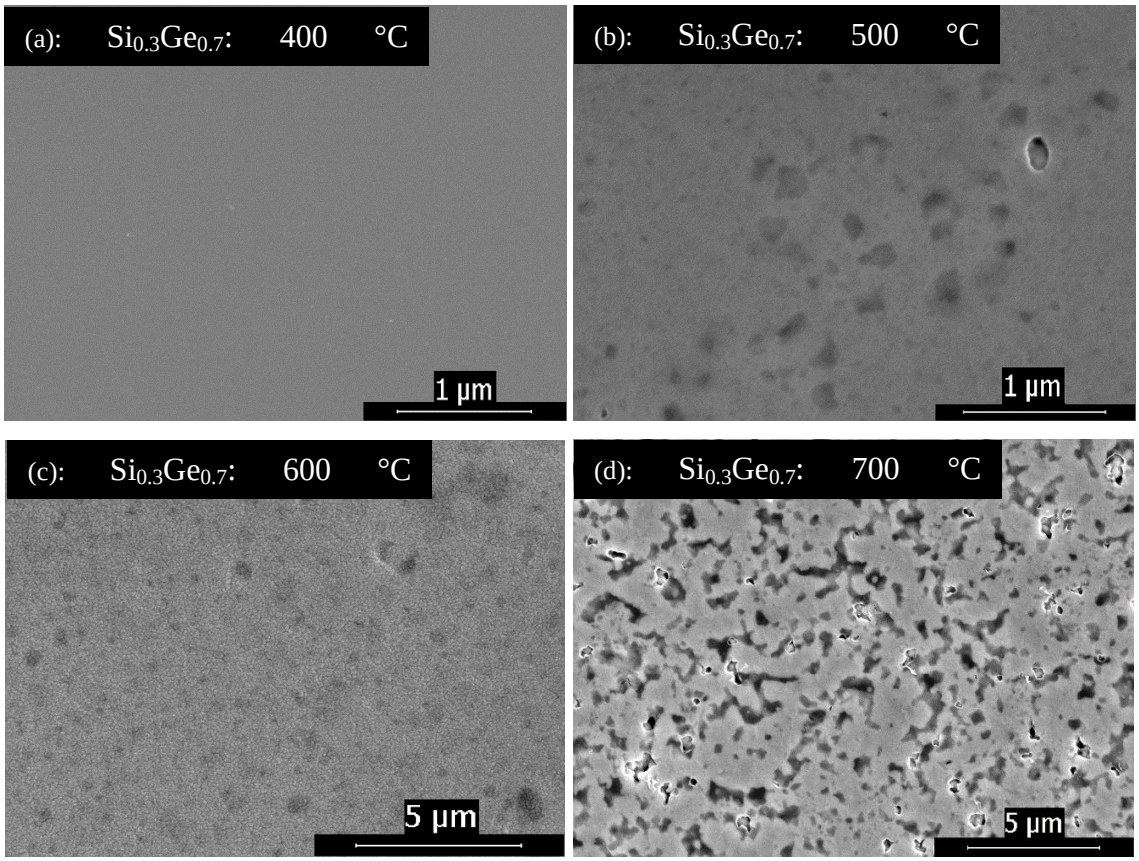

Figure 4. Surface morphology of the $Si_{0.3}Ge_{0.7}$ film after annealing at different temperatures, with a critical temperature for damage formation of 500 °C (see Figure 2(b)). Note the different magnification scales between images.

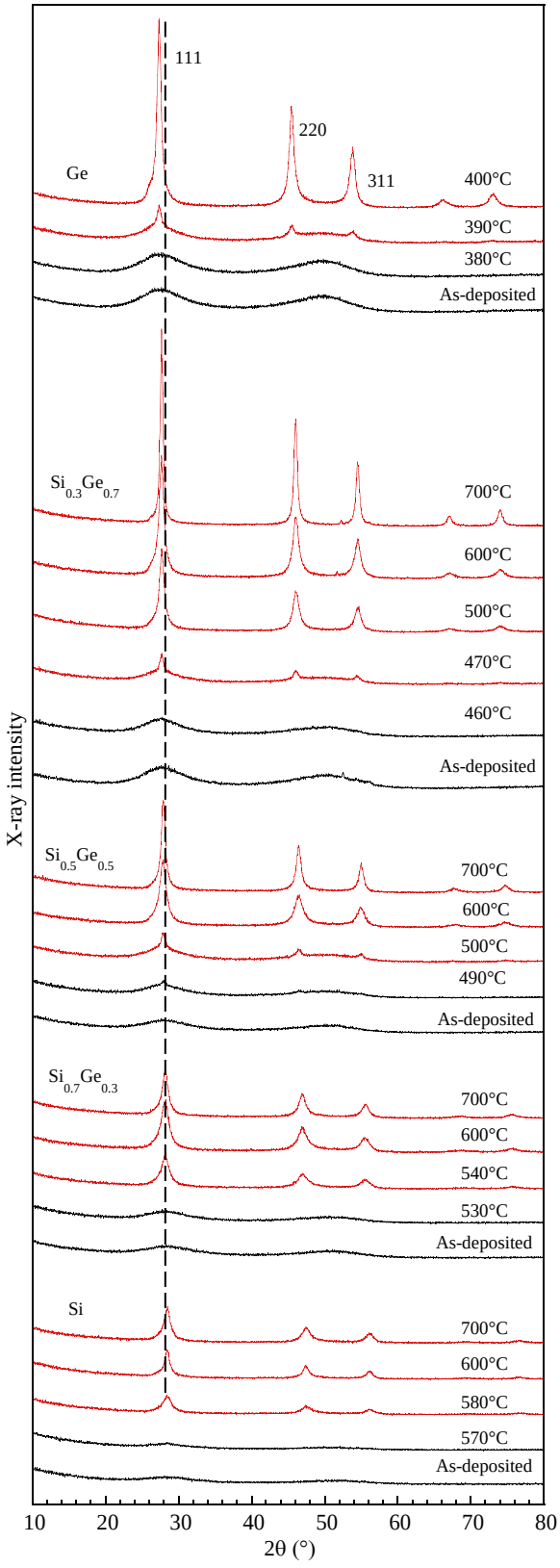

Figure 5. GIXRD patterns of $Si_{1-x}Ge_x$ thin films after annealing at different temperatures. The dashed line is used to indicate the shift in the 111 peaks for all films.

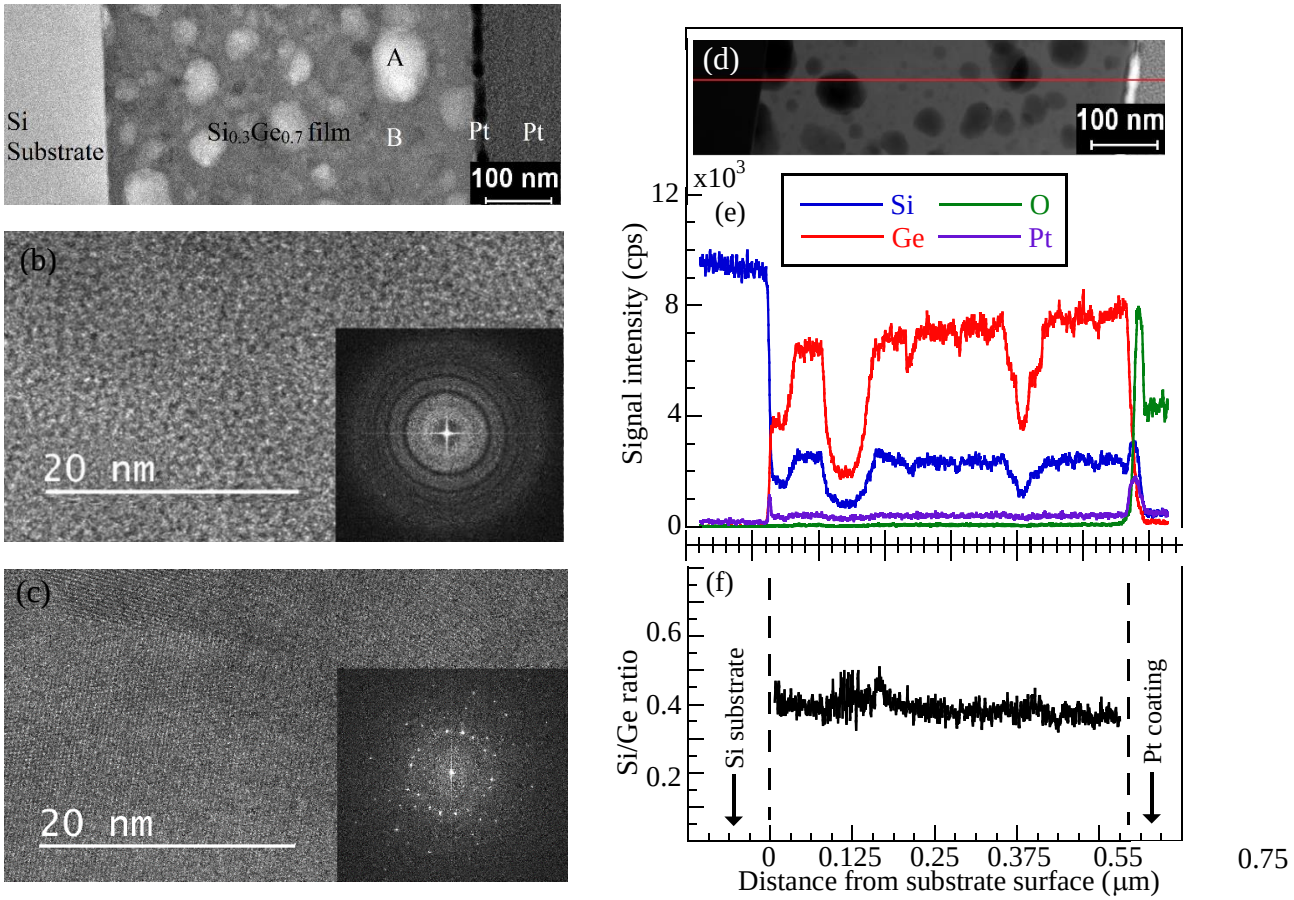

Figure 6. Cross-sectional TEM analysis of a $Si_{0.3}Ge_{0,7}$ film annealed at 600 °C. (a) Bright field TEM micrograph. (b) HRTEM micrograph of the amorphous white area in (a) with FFT image in the inset. (c) HRTEM micrograph of the crystalline dark area in (a) with FFT image in the inset. (d) HAADF image of the same sample and (e) EDS line scan of Si, Ge, O and Pt, and (f) a plot of Si to Ge ratio across the film.

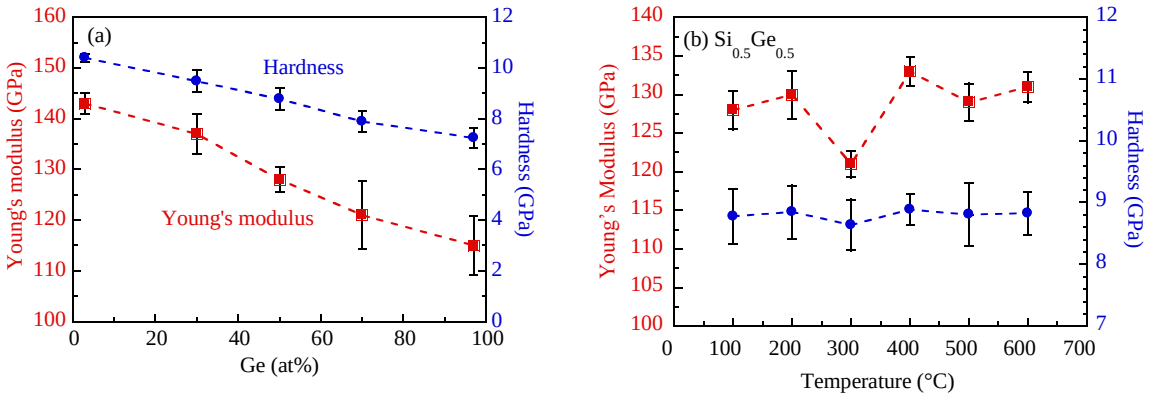

Figure 7. Young's modulus and hardness of (a) as-deposited $Si_{1-x}Ge_x$ films, and (b) as a function of annealing temperature for $Si_{0.5}Ge_{0.5}$, as determined by nanoindentation technique.

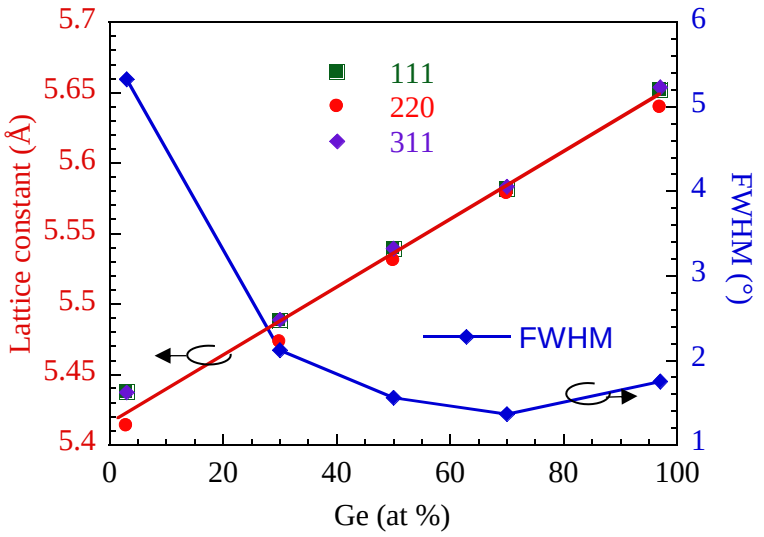

Figure 8. Lattice constant and FWHM of 111 XRD peaks for the $Si_{1-x}Ge_x$ thin films annealed at 700 °C (400 °C for the pure Ge sample) as a function of Ge content. The lines connecting the markers are simply a guide for the eye.

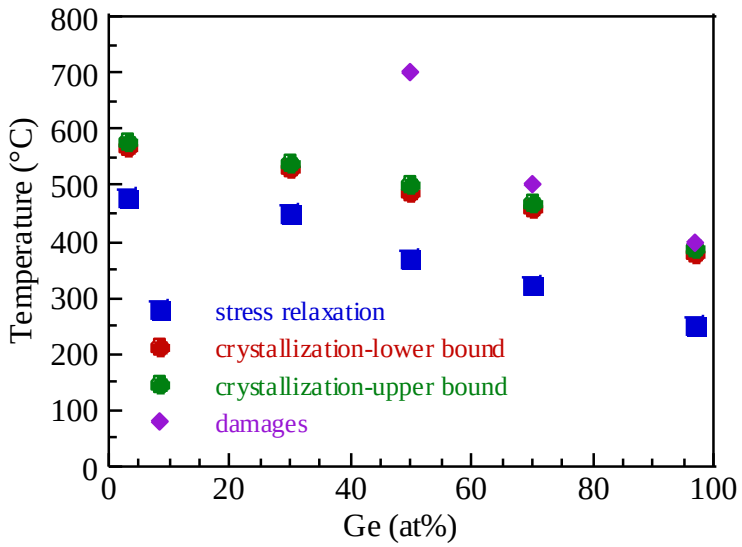

Figure 9. Characteristic annealing temperatures as a function of Ge content for (i) stress relaxation (square symbols), (ii) crystallisation (upper bound: green round symbols; lower bound: red round symbols) and (iii) physical damage (diamond symbols).

Table 1. Sample deposition parameters: target bias voltage = -800V, Ar flow rate = 53 sccm, target bias on/off time, film composition from EDS analysis, measured thin film thickness, Young's Modulus (E) and Hardness (H). Note that EDS analysis for film composition was normalised after excluding any Ar content.

Nominal film composition	Si target on/off time (μs)	Ge target on/off time (μs)	Thickness (nm)	EDS analysis ($Si_{1-x}Ge_x$)	Ar (%)	Young's Modulus (GPa)	Hardness (GPa)
Si	12/2	OFF	528	Si	4.0	143	10.4
$Si_{0.7}Ge_{0.3}$	12/2	2/26	515	$Si_{0.73}Ge_{0.27}$	4.0	137	9.48
$Si_{0.5}Ge_{0.5}$	12/2	10/18	533	$Si_{0.49}Ge_{0.51}$	4.0	128	8.78
$Si_{0.3}Ge_{0.7}$	12/2	27/1	576	$Si_{0.28}Ge_{0.72}$	4.0	121	7.89
Ge	OFF	26/2	527	Ge	4.0	115	5.77

Table 2. Young's modulus, atomic mass, Poisson's ratio, density and elastic energy of $Si_{1-x}Ge_x$ alloy as a function of x.

Properties	Equation	Source
Biaxial modulus, Y (GPa)	$Y = 180.45 - 39.96x$	[29], [30]
Atomic mass, M	$M = 28 \times (1 - x) + 32x$	Mass fraction
Poisson's ratios, ν	$\nu = 0.278 - 0.005x$	[3]
Density, D (g/cm^3)	$D = 2.329 + 3.493x - 0.499x^2$	[30]

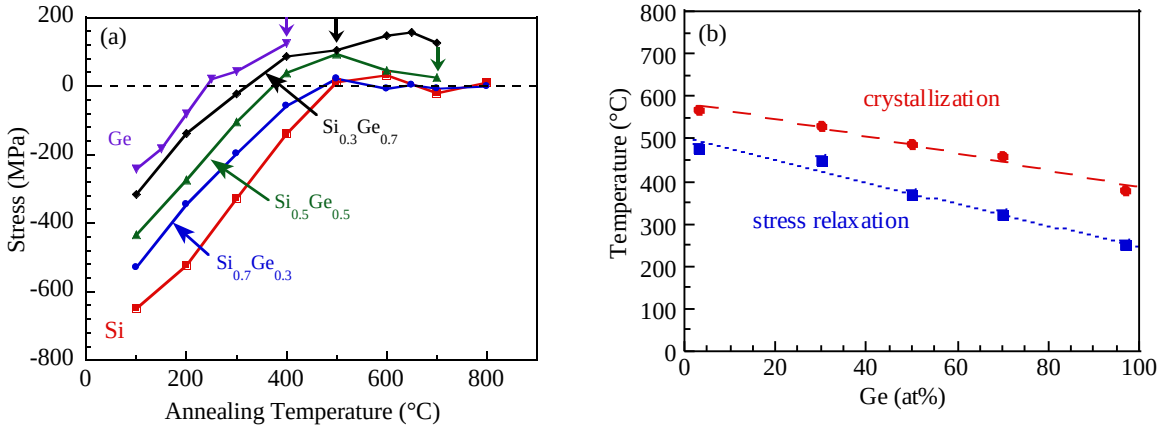

The as-deposited $Si_{1-x}Ge_x$ films contain in-plane compressive stresses. The stresses are relaxed upon annealing (Fig. a). The critical temperatures for stress relaxation and for crystallization decrease with increasing the Ge content of the films (Fig. b).